

# Electric field and surface charge effects on ferroelectric domain dynamics in BaTiO<sub>3</sub> single crystal

D. Y. He,<sup>1</sup> L. J. Qiao,<sup>1,\*</sup> Alex A. Volinsky,<sup>1,2</sup> Y. Bai,<sup>1</sup> and L. Q. Guo<sup>1</sup><sup>1</sup>*Corrosion and Protection Center, Key Laboratory for Environmental Fracture (MOE), University of Science and Technology Beijing, Beijing 100083, People's Republic of China*<sup>2</sup>*Department of Mechanical Engineering, University of South Florida, Tampa, Florida 33620, USA*

(Received 24 December 2010; revised manuscript received 5 March 2011; published 1 July 2011)

The potential distribution of BaTiO<sub>3</sub> single crystal ferroelectric domains was investigated by scanning Kelvin probe microscopy at room temperature with and without an electric field applied parallel to the (001) top surface. Immediate  $c$  domain surface potential inversion was observed after reaching the 6 V/mm critical electric field intensity followed by complete recovery upon switching the electric field off. Piezoresponse force microscopy was used to characterize domain structure evolution during the electric field application, which caused  $c$  domain motion. Newly formed domain patterns were stable for a month after switching the electric field off. Screening surface charges and their mobility play a dominant role in this experiment.

DOI: [10.1103/PhysRevB.84.024101](https://doi.org/10.1103/PhysRevB.84.024101)

PACS number(s): 77.80.Dj, 77.80.Fm, 68.43.-h, 68.37.Ef

## I. INTRODUCTION

Ferroelectric perovskite oxide domain patterns are related to spontaneous polarization.<sup>1</sup> Screening of surface charges is a crucial phenomenon in ferroelectrics. Spontaneous polarization and the surface charge are related, thus domain charges are reflected in surface potential images.<sup>2</sup> Scanning probe microscopy (SPM) is a powerful tool for observing domain structures and their dynamic behavior in ferroelectric materials at micron and nanometer scales.<sup>3-9</sup> As a simple and convenient nondestructive method, SPM can be used to observe ferroelectric domain dynamics. Among SPM modes, scanning Kelvin probe microscopy is sensitive to an electrostatic force that can be directly used to detect surface potential distribution on ferroelectric surfaces *in situ*.<sup>10,11</sup> Based on the piezoelectric effect, piezoresponse force microscopy (PFM) is used to characterize domain structures.<sup>12-14</sup> The main function of PFM is to detect and map local deformation, within the sample, in response to a bias applied to the tip, thereby providing valuable insight into the domain characteristics. These two modes are useful for characterizing ferroelectric domain polarization. Both Kelvin probe microscopy and PFM were used in experiments described in this paper while applying an electric field to the sample.

Domain scanning probe imaging and measurements of the surface potential in ferroelectrics have been carried out by many researchers.<sup>15-25</sup> These studies primarily deal with the presence of adsorbates on perovskite surfaces and, consequently, observations of surface potential inversion have been reported by several investigations. Kalinin *et al.* reported temperature-induced potential inversion on the BaTiO<sub>3</sub> (001) single crystal surface.<sup>15</sup> Liu *et al.* also observed surface potential inversion after heating a LiNbO<sub>3</sub> single crystal.<sup>16</sup> Bonnell *et al.* reported surface charge effects on the characterization of the domain polarization surface potential and the domain destabilization measured by PFM.<sup>17</sup> This demonstrates that charges are screened on polarized ferroelectric surfaces and that surface charge dynamics affect the domain electric performance. The influence of surface adsorbates should also be taken into account.

Here, surface potential inversion of ferroelectric domains in BaTiO<sub>3</sub> single crystal, upon applying a parallel electric field, is reported. This phenomenon was observed in ferroelectric  $c$  domains with their spontaneous polarization pointing either up or down, with respect to the top (001) surface. In this case surface charges migrated upon being driven by an applied electric field. Their domain polarization was then obtained from surface potential imaging. The research objective was to verify whether the observed surface potential inversion was related to the actual domain switching or the surface adsorbates screening. PFM was also used to characterize domain evolution during the electric field application.

## II. EXPERIMENTAL DETAILS

A BaTiO<sub>3</sub> single crystal with 4×3×1 mm<sup>3</sup> dimensions was used in this study. The crystal was poled along the [100] direction to get  $a$  domains on the observed (001) plane. The (001) surface was then polished with diamond lapping pastes, and a 50 nm colloidal silica suspension, until the surface roughness was less than 1 nm. The sample was then cleaned supersonically in deionized water for 100 s. After that, to obtain a multidomain structure, the BaTiO<sub>3</sub> crystal was heated to 135°C for 30 min in air, above its 120°C Curie temperature, and then cooled down to room temperature. This way, a BaTiO<sub>3</sub> polarized domain structure, containing  $a$ ,  $c^+$ , and  $c^-$  domains, was achieved.

Surface potential measurements were carried out with Digital Instruments Dimension V SPM (USA) utilizing W<sub>2</sub>C coated tip (NSG01/W<sub>2</sub>C, NT-MDT, Russia). Experiments were performed at 135 kHz, just below the 150 kHz cantilever resonance frequency. The lift scan height in the interleave control was set to 100 nm. An oscillating voltage  $V_{ac}\cos(\omega t)$  was applied directly to the cantilever tip to measure the surface potential. In these studies, the driving voltage  $V_{ac}$  was 1.5 V, with the scan rate of 1 Hz. Thus, it took 10 min to finish a complete surface potential image capture. In case of PFM, the same conductive tip was used. The PFM mode is based on an AFM contact mode, where the probe stays in permanent

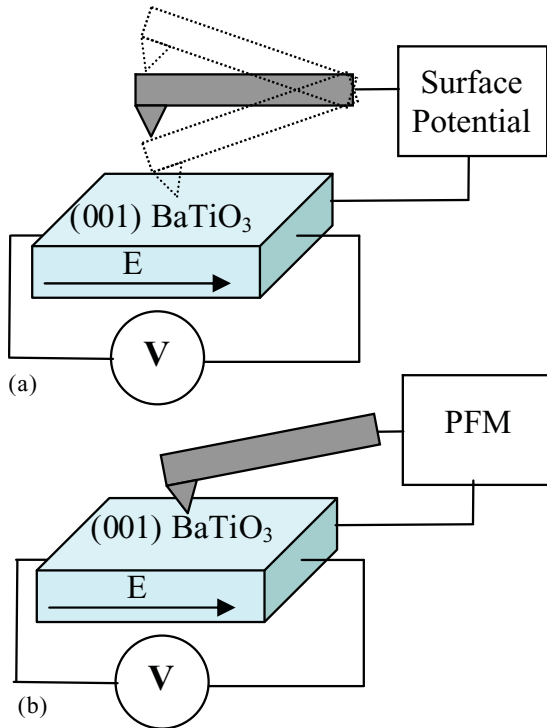


FIG. 1. (Color online) (a) Schematic of the surface potential measurements with electric field applied along the (001) BaTiO<sub>3</sub> surface. (b) Schematic of PFM measurements.

contact with the sample surface during imaging. To avoid damage to the tip, or the sample, a  $-0.2$  V setpoint was used. This corresponds to the  $364 \pm 42$  nN tip-surface force, and is high enough to measure semiconductor I-V characteristics.<sup>18</sup> A 10 V peak-to-peak AC signal was then applied between the probe and the sample at a 15 kHz frequency, providing the best image contrast. Mapping of the sample piezoelectric oscillation in response to the externally applied electric field, was done so by the lock-in amplifier. Domains with different orientations exhibited different vibration behavior, thereby distinguishing themselves from the contrast in piezoresponse images. The scan rate was 0.5 Hz, and it took 10 min to finish the whole image capture.

In this work, an external electric field ( $E_0$ ) was applied paralleled to the (001) top surface. Surface potential and PFM measurements were conducted while applying a different electric field. Fig. 1 shows schematics of the surface potential and PFM modes, respectively. By coating silver paste electrodes on both sides of the sample, a voltage source was connected using copper wires. Surface potential and PFM signals were measured to obtain local domain polarization evolution relative to the applied electric field in each mode, respectively.

### III. RESULTS AND DISCUSSION

Figures 2(a) and 2(b) show topography and surface potential maps of the BaTiO<sub>3</sub> (001) surface, respectively. Topography with corrugations is attributed to adjacent  $a$  and  $c$  domains. The  $90^\circ$   $a$ - $c$  domain walls appear as vertical straight lines on the surface. The  $c$  domain polarization charge is generated on the surface and has a polarization vector pointing either up

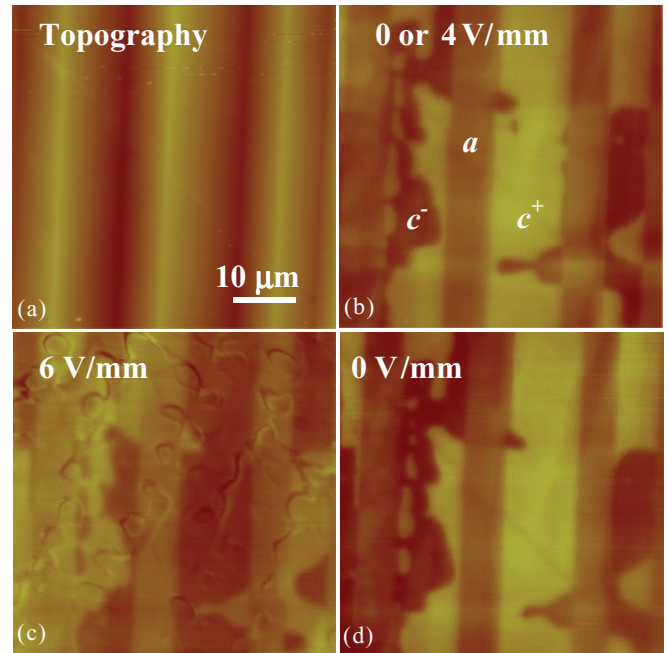


FIG. 2. (Color online) (a) AFM local topography image of the (001) BaTiO<sub>3</sub> surface with a 200 nm Z scale. (b) Surface potential image without voltage applied or with a 4 V/mm applied electric field intensity. (c) Surface potential image after applying a 6 V/mm electric field intensity showing surface potential inversion. (d) Complete recovery on switching the electric field off.

( $c^+$ ) or down ( $c^-$ ), with respect to the (001) plane. Dark regions within the  $c$  domain with a negative potential correspond to  $c^-$  domains, while the surrounding bright regions with positive potential correspond to  $c^+$  domains. The  $180^\circ$   $c^+$  and  $c^-$  domains are separated by irregular curved domain walls, while there is no difference between  $c^+$  and  $c^-$  domains observed in topography images. For the  $a$  domain, the polarization vector is in the (001) plane, thus it has no surface charge. It is, therefore, at zero potential and its contrast is between the  $c^+$  and  $c^-$  domains. Bright, dark, and intermediate regions correspond to the  $c^-$ ,  $c^+$ , and  $a$  domains, respectively, as marked in Fig. 2(b). By measuring the surface potential magnitude, one can calculate the surface potential difference between  $c^+$  and  $c^-$  domains of 100 mV.

An AFM topography image of the BaTiO<sub>3</sub> single crystal used in these experiments is shown in Fig. 2(a). It is worth noting that during testing local topography images did not change at all. Local surface potential images captured while applying 4 V/mm and 6 V/mm electric field intensity are shown in Fig. 2(b) and Fig. 2(c), respectively. Figure 2(b) with a 4 V/mm applied electric field intensities looks exactly the same as the original surface potential distribution, without an electric field applied. Gradually increasing the electric field intensity to 4 V/mm did not cause any changes. Continued scanning was conducted for 1 h for each applied electric field value. Then, the applied electric field intensity was continuously increased until it reached 6 V/mm. At that time, measured  $c$  domain surface potential inverted its sign, as seen in Fig. 2(c). A complete  $c$  domain sign inversion was observed. The ripples in Fig. 2(c) are simply noise caused by the applied electric field

and are not related to the intrinsic domain structure, as they change orientation with the scanning direction. Variation of the surface potential is seen by comparing Fig. 2(b) and 2(c), where positive charge areas (bright zones) become negative (dark zones), although the potential magnitude was much lower than the original value. Above this critical 6 V/mm electric field intensity value, up to 8 V/mm, no further change in the surface potential was observed.

It appears that a complete sign change of  $c^+$  and  $c^-$  domains occurred as if they had switched places with each other. It is important to understand the typical domain switching behavior. New domains can nucleate and polarized domains can change their orientation due to external loading in terms of an external electric field or stress. Based on a previous domain switching study,<sup>26</sup> it is typically accompanied by a domain nucleation and growth process after reaching a 200 V/mm coercive field intensity. However, during this 6 V/mm applied electric field surface potential measurement, domain switching happened in a very short time without domain wall movement, as seen from the potential mapping in Fig. 2(c). Here, surface potential inversion did not follow typical domain switching mechanisms. Thus, it is evident that the surface potential inversion did not happen because of the actual domain switching, but because reflects surface charges, related to surface polarization switched.

Based on X-ray photoelectron spectroscopy and PFM measurements, the BaTiO<sub>3</sub> surface layer consists of chemisorbed and physisorbed species.<sup>27</sup> One way to remove adsorbates is to heat the sample to relatively high temperatures. However, complete removal of adsorbates from the BaTiO<sub>3</sub> surface is impossible.<sup>27</sup> Defects, such as O vacancies, are preferred chemisorption locations.<sup>23</sup> Strong chemical bonds with both BaO and TiO<sub>2</sub> terminations also induce chemisorption. Geneste and Dkhil found, through density-functional calculations, that an in-plane-polarized BaTiO<sub>3</sub> (001) surface has strong interactions with water, chemisorbed on both BaO and TiO<sub>2</sub> terminations.<sup>28</sup> Thus, on the BaTiO<sub>3</sub> surface, strong interactions and immobile chemisorption happen by electron transfer of a chemical bond. On the other hand, highly mobile surface screening charges appeared due to physisorption on the polarized domain surface, reducing the depolarization field.<sup>29</sup> They are adsorbed on the surface by means of attractive forces from oriented dipoles, as similarly found in our previous study of water adsorption on a BaTiO<sub>3</sub> single crystal.<sup>30</sup> These attractive forces have a strong effect on the spread of the ferroelectric surface charge. Adsorbed charges on the oxide surface are removable. The low activation energy of 4 kJ/mole<sup>15</sup> suggests that, regardless of the interaction between adjacent screening charges, the energy of a single mobile charge is only 0.04 eV. Thus, immediate desorption can easily happen due to an applied electric field and consequently, charge diffusion process was observed. At any point of the image the effective electric field,  $E_{\text{eff}}$ , can be estimated as:

$$E_{\text{eff}} = E_0 + E_a + E_d \quad (1)$$

Here,  $E_0$  is an externally applied electric field,  $E_a$  is an intrinsic field related to the ferroelectric symmetry breakdown, or anisotropy field, and  $E_d$  is a depolarizing field induced by bound charges. Thus, the obtained effective electric field is

dramatically decreased compared with the externally applied electric field. In our test, the 6 V/mm applied electric field intensity was reduced to 2 V/mm, based on the actual surface potential measurements. Although a 6 V/mm reversal electric field intensity is low compared with a 200 V/mm coercive field intensity,<sup>31,32</sup> the effective electric field is still sufficient to mobilize part of screening charges on the surface. Although physisorbed species are removed, chemisorbed charges stay on the surface to compensate depolarizing field. Immobile charges or adsorbates remain on the surface to compensate the polarized state. When the electric field is switched off, surface compensation returns to the charge screening state. Again, surface potential recovers to the original value, since the electric field-dependent surface potential mainly relies on the adsorption and desorption of the surface screening charges.

As an alternative explanation, it has been reported that stable domain polarization distribution would not change until the surface compensation charge density exceeds a critical 0.7–0.8 C/m<sup>2</sup> value based on the phase field model.<sup>33</sup> During the experiment, after the mobile charges detached from the surface while the electric field was applied, the surface charge screening state was changed. In the absence of mobile charges, the surface charge density decreased to a partially screened state. As a result, the measured surface potential sign was reversed. However, after mobile charges were removed, the charge density still did not pass the critical value that could still sustain the original domain polarization by compensation of the ferroelectric surface, thus, no domain wall movement was observed and no new domains appeared.

In order to understand the behavior of mobile charges on a ferroelectric surface, PFM was utilized to characterize the surface charge dynamic effects on ferroelectric domain inversion during electric field application. Continued scanning was conducted for 1 h for each value of the applied electric field. After 1 h of scanning without an applied electric field, no changes appeared in the PFM images. After 1 h of testing, with an applied electric field intensity of 2 V/mm, there was still no change in domain structure. When the applied electric field intensity was increased to 4 V/mm, no obvious changes occurred during the first 20 min. Consequently, the  $c$  domain structure gradually changed with time. The 180°  $c$  domain wall was removed. After 90 min of scanning the  $c$  domain structure had changed significantly, whereas the  $a$  domain did not change throughout the whole scanning period. Another  $a$ - $c$  domain area was selected for PFM scanning and, with a 6 V/mm applied electric field intensity, the PFM image changed more dramatically as can be seen in Fig. 3. After only three complete image captures in 30 min, all  $c^+$  domains changed to  $c^-$  domains. While a significant  $c$  domain mobility was observed, the  $a$  domain did not change. Bonnell *et al.* found that under UV illumination domain walls moved rapidly during PFM scanning.<sup>17</sup> We observed the same behavior when a parallel electric field was applied to the sample during PFM scanning. Furthermore, inspection of a larger image of the measured zone in Fig. 3(d) reveals that the domain motion is mainly induced by the tip scanning, since only the previously scanned area, underneath the tip, was involved in the domain evolution. An obvious square in the middle of Fig. 3(d) is the scanning area where PFM measurements were performed earlier. The larger area outside of the previously scanned

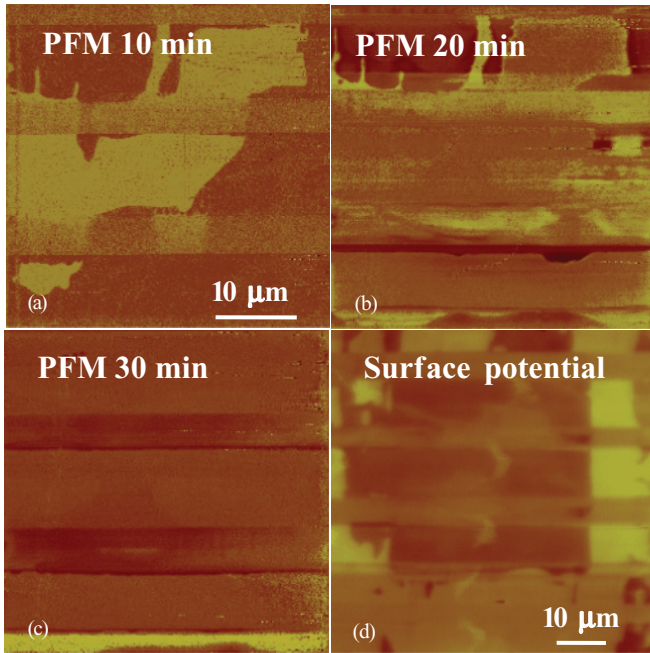


FIG. 3. (Color online) PFM images of domain structure on (001) BaTiO<sub>3</sub> single crystal showing domain evolution with a 6 V/mm electric field intensity applied to the sample for (a) 10 min, (b) 20 min, and (c) 30 min. (d) Larger surface potential image showing a zoomed-out area.

square remains unmodified, exhibiting the same features as in the beginning of the experiment.

In Fig. 4, the  $c^+$  domain area dependence on scanning time at 4 V/mm and 6 V/mm is plotted, showing the  $c^+$  domain switching to the  $c^-$  domain. Domain evolution was more rapid with a higher applied electric field. After switching the electric field off, the newly achieved  $a$ - $c$  domain structure was stable and did not change, even after 1 month of storage.

When an electric field was applied, it stimulated the surface screening charge on the polarized  $c$  domain, leading to surface charge migration. During PFM imaging, the AFM tip, with a conductive coating, stays in contact with the surface. Removed mobile charges migrated along the tip and gathered at the end of the tip. Thus, a high local electric field was formed between the tip and the sample. The higher 6 V/mm applied electric field intensity moved the screening charges more easily. So, in a very short time, the gathered charges formed a large enough local tip electric field, and lead to a faster and more dramatic domain motion, as compared to the lower 4 V/mm applied electric field intensity. In the case of 4 V/mm, the surface screening charges already possess a certain energy that does not exceed the physisorption energy and, therefore, fails to initiate potential switching. However, a conductive tip in contact with the ferroelectric surface stimulates the charges. Thus after 20 min of inactivity the domains start to move. Furthermore, at 4 V/mm the domain motion is much slower than at the 6 V/mm applied electric field intensity, as seen in Fig. 4. For the  $a$  domain, there is no screening charge on the surface. As a result, when the tip scanned the  $a$  domain region, there was no mobile screening charge gathered, even though an electric field was applied to the sample. Thus, no local electric field was generated between the tip and the sample, resulting in

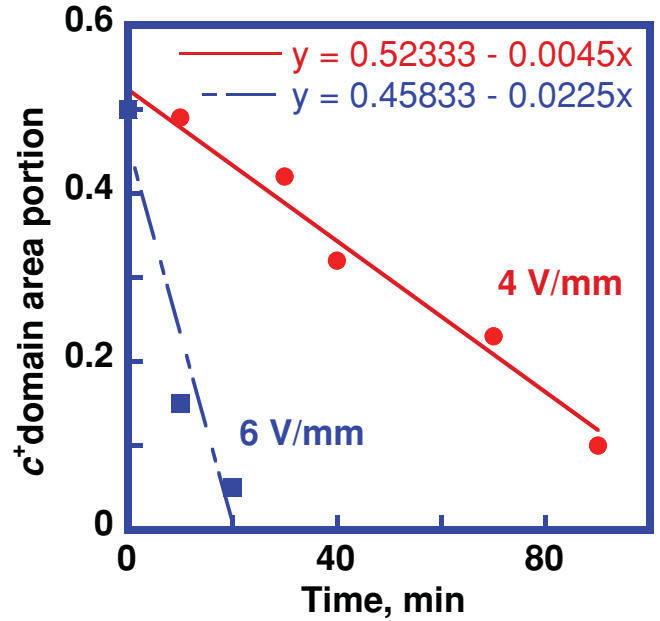


FIG. 4. (Color online) The  $c^+$  domain area portion of the total  $c$  domain area for the 4 V/mm and 6 V/mm applied electric field intensities. Originally the  $c^+$  domains occupied half of the  $c$  domain area and later switched to  $c^-$  domains.

no  $a$  domain change. It turns out that PFM scanning-induced domain evolution was related not only to the electric field applied to the sample, but also to the polarization state of the domain. Surface screening charges, and their mobility, play a dominant role in the described experiments.

#### IV. CONCLUSIONS

In summary, the surface potential evolution on the (001) BaTiO<sub>3</sub> single crystal surface, with electric fields applied along the [010] direction, was studied. A strong influence of the electric field on the surface potential of the BaTiO<sub>3</sub> domain was found. The surface potential sign of the  $c$  domains reversed as soon as an applied electric field intensity reached 6 V/mm and switched back after the electric field was turned off. This electric field-dependent surface potential mainly relies on the adsorption and desorption of the surface screening charges, which are driven by the low 4 kJ/mole activation energy. The potential exhibited inversion because of the surface charge dispersion. Domain motion induced by PFM scanning while applying an electric field, was caused by removing the screening charge accumulated at the end of the tip. A local electric field was generated between the tip and the sample. This led to domain evolution in PFM mode, where the conductive tip stayed in contact with the sample surface.

#### ACKNOWLEDGMENTS

Authors acknowledge support from the National Nature Science Foundation of China under Grants No. 51072021 and No. 50632010 and from Beijing Municipal Commission of Education under Grant No. YB20091000801. Alex Volinsky acknowledges support from the National Science Foundation under Grants No. 1000138 and No. 0966248.

- \*lqiao@ustb.edu.cn
- <sup>1</sup>D. Vanderbilt, *Phys. Rev. B* **41**, 7892 (1990).
- <sup>2</sup>S. V. Kalinin and D. A. Bonnell, *Phys. Rev. B* **63**, 125411 (2001).
- <sup>3</sup>Y. G. Wang, J. Dec, and W. Kleemann, *J. Appl. Phys.* **84**, 6795 (1998).
- <sup>4</sup>J. Munoz-Saldana, G. A. Schneider, and L. M. Eng, *Surf. Sci.* **480**, L402 (2001).
- <sup>5</sup>B. Reichenberg, S. Tiedke, K. Szot, F. Peter, R. Waser, S. Tappe, and T. Schneller, *J. Eur. Ceram. Soc.* **25**, 2353 (2005).
- <sup>6</sup>B. J. Rodriguez, R. J. Nemanich, A. Kingon, and A. Gruverman, *Appl. Phys. Lett.* **86**, 012906 (2005).
- <sup>7</sup>Y. B. Park, M. J. Dicken, Z. H. Xu, and X. D. Li, *J. Appl. Phys.* **102**, 083507 (2007).
- <sup>8</sup>O. S. Ovchinnikov, S. Jesse, and S. V. Kalinin, *Nanotechnology* **20**, 255701 (2009).
- <sup>9</sup>S. V. Kalinin, A. N. Morozovska, L. Q. Chen, and B. J. Rodriguez, *Rep. Prog. Phys.* **73**, 056502 (2010).
- <sup>10</sup>Q. Zhang, C. H. Kim, Y. H. Jang, H. J. Hwang, and J. H. Cho, *Appl. Phys. Lett.* **96**, 152901 (2010).
- <sup>11</sup>Y. Kim, M. Park, S. Buhlmann, S. Hong, Y. K. Kim, H. Ko, J. Kim, and K. No, *J. Appl. Phys.* **107**, 054103 (2010).
- <sup>12</sup>F. Peter, A. Rüdiger, and R. Waser, *Rev. Sci. Instrum.* **77**, 036103 (2006).
- <sup>13</sup>A. N. Morazovska, E. A. Eliseev, and S. V. Kalinin, *J. Appl. Phys.* **102**, 074105 (2007).
- <sup>14</sup>T. Jungk, Á. Hoffmann, and E. Soergel, *Appl. Phys. Lett.* **89**, 163507 (2006).
- <sup>15</sup>S. V. Kalinin, C. Y. Johnson, and D. A. Bonnell, *J. Appl. Phys.* **91**, 3816 (2002).
- <sup>16</sup>X. Y. Liu, K. Kenji, and T. Kazuya, *Appl. Phys. Lett.* **89**, 132905 (2006).
- <sup>17</sup>R. Shao, M. P. Nikiforov, and D. A. Bonnell, *Appl. Phys. Lett.* **89**, 112904 (2006).
- <sup>18</sup>M. Li, Y. J. Su, W. Y. Chu, L. J. Qiao, A. A. Volinsky, and G. Kravchenko, *Appl. Phys. Lett.* **98**, 082105 (2011).
- <sup>19</sup>Q. Dai, J. Hu, and M. Salmeron, *J. Phys. Chem. B* **101**, 1994 (1997).
- <sup>20</sup>M. Luna, J. Colchero, and A. M. Baro, *J. Phys. Chem. B* **103**, 9576 (1999).
- <sup>21</sup>M. Luna, J. Colchero, A. Gil, J. Go'mez-Herrero, and A. M. Baro, *Appl. Surf. Sci.* **175**, 393 (2000).
- <sup>22</sup>A. Verdager, M. Cardellach, and J. Fraxedas, *J. Chem. Phys.* **129**, 174705 (2008).
- <sup>23</sup>D. B. Li, M. H. Zhao, J. Garra, A. M. Kolpak, A. M. Rappe, D. A. Bonnell, and J. M. Vohs, *Nat. Mater.* **7**, 473 (2008).
- <sup>24</sup>S. V. Kalinin and D. A. Bonnell, *Appl. Phys. Lett.* **78**, 1116 (2001).
- <sup>25</sup>S. Shin, J. Baek, J. W. Hong, and Z. G. Khim, *J. Appl. Phys.* **96**, 4372 (2004).
- <sup>26</sup>B. Jiang, Y. Bai, W. Y. Chu, and L. J. Qiao, *Appl. Phys. Lett.* **93**, 152905 (2008).
- <sup>27</sup>F. Peter, K. Szot, R. Waser, B. Reichenberg, S. Tiedke, and J. Szade, *Appl. Phys. Lett.* **85**, 2896 (2004).
- <sup>28</sup>G. Geneste and B. Dkhil, *Phys. Rev. B* **79**, 235420 (2009).
- <sup>29</sup>S. V. Kalinin and D. A. Bonnell, *J. Appl. Phys.* **87**, 3950 (2000).
- <sup>30</sup>D. Y. He, L. J. Qiao, A. A. Volinsky, Y. Bai, M. Wu, W. Y. Chu, *Appl. Phys. Lett.* **98**(6), 062905 (2011).
- <sup>31</sup>W. J. Merz, *Phys. Rev.* **95**, 650 (1954).
- <sup>32</sup>A. Ryuji, *J. Phys. Soc. Jpn.* **15**, 795 (1960).
- <sup>33</sup>J. Wang and M. Kamlah, *Appl. Phys. Lett.* **93**, 262904 (2008).